

# A shallow water model for MHD flows with turbulent Hartmann layers

Alban Pothérat and Jean-Philippe Schweitzer  
Coventry University, Applied Mathematics Research Centre,  
Priory Street Coventry CV1 5FB, United Kingdom \*  
(Dated: 4 April, 2011)

We establish a shallow water model for flows of electrically conducting fluids in homogeneous static magnetic fields that are confined between two parallel planes where turbulent Hartmann layers are present. This is achieved by modelling the wall shear stress in these layers using the Prandtl's mixing length model, as did the authors of [15]. The idea for this new model arose from the failure of previous shallow water models that assumed a laminar Hartmann layer to recover the correct amount of dissipation found in some regimes of the MATUR experiment. This experiment, conducted by the authors of [2], consisted of a thin layer of mercury electrically driven in differential rotation in a transverse magnetic field. Numerical Simulations of our new model in the configuration of this experiment allowed us to recover experimental values of both the global angular momentum and the local velocity up to a few percent when the Hartmann layer was in a sufficiently well developed turbulent state. We thus provide an evidence that the unexplained level of dissipation observed in MATUR in these specific regimes was caused by turbulence in the Hartmann layers. A parametric analysis of the flow, made possible by the simplicity of our model, also revealed that turbulent friction in the Hartmann layer prevented quasi-2D turbulence from becoming more intense and limited the size of the large scales.

## I. INTRODUCTION

Geophysical and astrophysical flows such as planetary atmospheres, oceans and accretion disks are, to a large extent, governed by 2D dynamics, and have been providing a continuous incentive to study 2D flows for decades. From the theoretical point of view, 2D flows in general and 2D turbulence in particular offer a realistic and more accessible alternative to their 3D counterpart, both in terms of complexity and computational costs. Achieving flows with purely 2D dynamics in an experiment, however, presents somewhat of a challenge, because in the laboratory, nothing is ever quite 2D. A promising solution emerged when quasi-2D flows were reproduced in small scale laboratory experiments (10-20 cm) by imposing a strong enough homogeneous static magnetic field ( $B \gtrsim 0.1$  T) across a thin layer of liquid metal (thickness  $H \sim 1$  cm). The layer was either confined between two walls, or between a wall and a free surface, as in Lehnert's experiment [3] which was probably the first of this kind. In this class of experiments, the flow was never strong enough to affect the externally imposed magnetic field [4]: the main electromagnetic effect was that of the Lorentz force, which diffused the momentum along the field lines. For a given structure of size  $l_{\perp}$  and velocity  $U_L$ , diffusion was achieved over the entire channel width  $H$  in typical time  $\tau_{2D} = \rho/(\sigma B^2)(H/l_{\perp})^2$  [5] ( $\rho$  and  $\sigma$  are the fluid density and electrical conductivity). Even for moderately intense flows, this time was much shorter than the typical structure turnover time  $l_{\perp}/U_L$ , so physical quantities were indeed invariant across the channel, except in the boundary layers along the channel walls, called Hartmann layers.

Because of them, this class of flow is not strictly 2D but only *quasi-2D*, and requires dedicated models, such as the SM82 model formulated by [5]. This model was obtained following the shallow-water approach, a popular technique to model geophysical flows [6]. The idea of shallow water models is that when physical quantities vary little in one of the directions of space (here  $\mathbf{e}_z$ ), the fluid motion mostly takes place in the other two so it is still well represented by averaging the governing equations along the short dimension [6]. Theory and numerical simulations based on the SM82 model could finely reproduce the details of quasi-2D flows observed in experiments, as long as outside of the boundary layers, the momentum diffusion along the magnetic field lines acted much faster than 3D inertia and viscous friction. The ratios of these effects are respectively measured by two non-dimensional numbers: the 'true' interaction parameter introduced by [9],  $N_t = N(l_{\perp}/H)^2$ , and the square of the Hartmann number  $Ha = BH(\sigma/(\rho\nu))^{1/2}$ . Here the interaction parameter  $N = \sigma B^2 H/(\rho U)$ , where  $U$  is a typical fluid velocity is based on the same lengthscale as the Hartmann number for convenience. In these notations, the ratio of the Lorentz force to 2D inertia in the core of quasi-2D flows such as those we are interested in is of the order of  $(N/Ha)(l_{\perp}/H)$ , whereas in the Hartmann layer, it becomes of the order of  $N(l_{\perp}/H)$  [5, 10]. The MAGnetic TURbulence (MATUR) experiment in Grenoble [7, 8], was an experiment where these conditions were well satisfied. Over the years, its successive versions have been providing a wealth of reference data that have motivated the development of models for MHD and quasi 2D flows: most recently, [11] proposed a model for quasi-2D turbulence under high magnetic fields, based on SM82. MATUR consisted of a thin, cylindrical container filled with mercury placed in a transverse magnetic field (figure 2), where a circular,

\* alban.potherat@coventry.ac.uk

turbulent shear layer was generated by electrically driving into rotation the outer region of the cylindrical fluid domain [1]. When  $Ha \gg 1$  and  $N(l_{\perp}/H) \gg 1$ , the Hartmann boundary layers that confined the flow were laminar, with a simple exponential profile, as assumed in SM82. For  $N(l_{\perp}/H) \simeq 1$ , however, both global and local recirculations at the scale of individual vortices appeared. They transferred angular momentum to the side layers at the outer edge of the container where an extra dissipation took place that SM82 could not account for. This was later corrected in the more refined PSM model [10]. This new model included inertia in the Hartmann layers, which was responsible for these recirculations and was able to accurately reproduce experimental results in these regimes [12]. One set of measurements remains, however, where both SM82 and PSM grossly underestimate the dissipation. In this regime,  $Ha \in \{132, 212\}$  and  $N(l_{\perp}/H) \gg 1$ , so the 3D recirculations described by PSM are too weak to produce the missing dissipation. The Reynolds number based on the Hartmann layer thickness  $R = UH/(2\nu Ha) = Re/(2Ha)$ , however, was over the value of 380, for which the Hartmann layer in a rectilinear channel flow becomes turbulent [13, 14]. In spite of the difference between this ideal configuration and MATUR, it is tempting to think that the missing dissipation could be found in turbulent Hartmann layers.

In this paper, we explore this possibility by building a 2D model based on the assumption of a turbulent Hartmann layer. We shall proceed as follows: we first recall the general form of 2D MHD models. We then insert the model for turbulent Hartmann layers derived by [15] in this general form to obtain our particular model (section II). We then turn our attention to MATUR where we obtain a first estimate for the global angular momentum out of an axisymmetric version of our new model (section III). Finally, we implement our model in the code we previously used to simulate the SM82 and PSM equations [12], and simulate the flow in MATUR in detail (section IV).

## II. MODEL EQUATIONS

### A. Shallow water models in Low- $Rm$ MHD

To establish the shallow water equations, we shall consider the generic configuration of an MHD channel flow: an electrically conducting fluid (density  $\rho$ , kinematic viscosity  $\nu$ , electrical conductivity  $\sigma$ ) is confined between two horizontal impermeable walls respectively located at  $z = -H/2$  and  $z = H/2$  and the whole fluid domain is subject to an externally applied homogeneous magnetic field  $B\mathbf{e}_z$ . We shall work under the low- $Rm$  approximation ( $Rm = \mu\sigma Ul_{\perp} \ll 1$ ) [4], valid for liquid metals flowing at moderate speeds and in moderately large fluid domains such as those encountered in many engineering and laboratory situations. Its main impli-

cation is that, although the electric current induced by the motion of conducting fluid in the magnetic field (or order  $\sigma BU$ ) cannot be neglected as it participates in the Lorentz force, the magnetic field induced by this current ( $\sim BRm$ ) is, by contrast, negligible. Consequently, the fluid motion is incapable of modifying the externally applied field and electromagnetic effects only appear through the Lorentz force in the momentum equations. Under this assumption, and normalising lengths by  $H$ , velocities by  $U$ , time by  $H/U$ , pressure by  $\rho U^2$ , shear stress by  $(\rho\nu U/H)Ha$  and electric current density by  $\sigma BU/Ha$ , the average along  $\mathbf{e}_z$  of the equations that express the conservation of momentum and mass can be written in non-dimensional form as [12]:

$$\begin{aligned} \partial_t \bar{\mathbf{u}}_{\perp} + \bar{\mathbf{u}}_{\perp} \cdot \nabla_{\perp} \bar{\mathbf{u}}_{\perp} + \overline{(\mathbf{u}' \cdot \nabla) \mathbf{u}'} + \nabla_{\perp} \bar{p} = \\ \frac{N}{Ha^2} \nabla_{\perp}^2 \bar{\mathbf{u}}_{\perp} + \frac{N}{Ha} (\bar{\mathbf{j}}_{\perp} \times \mathbf{e}_z) - 2 \frac{N}{Ha^2} \tau_W, \quad (1) \\ \nabla \cdot \bar{\mathbf{u}} = 0, \quad (2) \end{aligned}$$

where the over-bar denotes  $z$ -averaging across the fluid depth ( $z = -1/2$  to  $z = 1/2$ ),  $\mathbf{u}'$  represents the departure from the averaged velocity  $\bar{\mathbf{u}}$ , and  $\tau_W(x, y)$  is the friction at a single Hartmann wall. At this point, the velocity scale  $U$  is left unspecified to keep the generality of the model, but will be assigned a value in section III for the particular case of the MATUR experiment. The governing parameters are the Hartmann number  $Ha = BH(\sigma/(\rho\nu))^{1/2}$  and the interaction parameter  $N = \sigma B^2 H/(\rho U)$  introduced in section I. Quantities averaged along  $z$  are by definition dependent only on  $x$  and  $y$ . The corresponding Nabla operator  $\nabla_{\perp}$  is 2D and carries the subscript  $(\ )_{\perp}$ . Similarly, the same subscript on a vector indicates components perpendicular to the magnetic field only.  $\bar{\mathbf{j}}_{\perp}$  can be expressed by averaging the equations governing the continuity of electric current and Ohm's law:

$$\nabla_{\perp} \cdot \bar{\mathbf{j}}_{\perp} = -j_W, \quad (3)$$

$$\frac{1}{Ha} \bar{\mathbf{j}}_{\perp} = \bar{\mathbf{E}}_{\perp} + \bar{\mathbf{u}}_{\perp} \times \mathbf{e}_z, \quad (4)$$

where  $j_W$  is the current density injected at one or both of the confining planes and  $\bar{\mathbf{E}}$  is a non-dimensional electric field. Taking the curl of the Ohm's law and using the incompressibility condition, one sees that  $\bar{\mathbf{j}}_{\perp}$  is irrotational. It follows that there is a potential  $\psi_0$  for  $\bar{\mathbf{j}}_{\perp}$  which satisfies Poisson's equation, the source term being  $j_W$ :

$$\bar{\mathbf{j}}_{\perp} = \nabla_{\perp} \psi_0, \quad \nabla_{\perp}^2 \psi_0 = -j_W. \quad (5)$$

The potential  $\psi_0$  is determined from the current source as the solution of Poisson's equation (5), which is unique for given boundary conditions for the electric current at the lateral boundaries. Then, using the vector field  $\mathbf{u}_0$  of streamfunction  $\psi_0$ , the Lorentz force in equation (1) turns out to be only determined by the boundary condition on the electric current through (5) and  $\bar{\mathbf{j}}_{\perp} \times \mathbf{e}_z = \mathbf{u}_0$ . At this point, the equations have been simply averaged,

and no assumption has been added to the Navier-Stokes equations. To complete the construction of a 2D model the averaged equations must be closed by the addition of a model for the inertial term  $(\mathbf{u}' \cdot \nabla) \mathbf{u}'$  as well as for the wall friction term  $\tau_W$  in (1).

## B. Model for flows with turbulent Hartmann layers

To model the MATUR experiment in regimes where the Hartmann layer is thought to be turbulent, we shall require two additional assumptions. The first one applies to the core of the flow, precisely outside of the Hartmann layer (a rigorous definition of this notion can be found in [16]). There, we shall still assume that the diffusion of momentum along the magnetic field lines by the Lorentz force dominates viscous and 3D inertial effects outside boundary layers, which is valid in the limit:

$$Ha \gg 1, \quad N_t = N \left( \frac{l_\perp}{H} \right)^2 \gg 1. \quad (6)$$

The true interaction parameter  $N_t$  introduced by [9], represents the effective ratio of the momentum diffusion along magnetic field lines due to the Lorentz force, to inertia, as discussed in introduction. In this limit, the pressure and the velocity components across the magnetic field are invariant in the  $z$  direction, outside the Hartmann layers. These assumptions are often referred to as the 2D core flow approximation [17]. Recently, we have been able to actually observe this flow structure [18], as well as the conditions under which two-dimensionality breaks down [19] in regimes where the Hartmann layer was most likely laminar. Yet, in spite of strong theoretical and numerical support [14] in favour of the existence of flows where a turbulent Hartmann layers and a 2D core co-exist, their experimental evidence is still lacking. In a way, the 2D core approximation justifies the physical relevance of 2D models on account that if  $\delta$  denotes the thickness of the boundary layers along the channel walls, then the velocity outside them,  $\mathbf{u}^c$ , a quantity usually measured in experiments [20], is well approximated by the average velocity as  $\bar{\mathbf{u}} = \mathbf{u}^c + O(\delta/H) = \mathbf{u}^c + O(Ha^{-1})$ . This implies in particular that  $(\mathbf{u}' \cdot \nabla) \mathbf{u}' \sim (\delta/H)^2 \bar{\mathbf{u}}_\perp \cdot \nabla_\perp \bar{\mathbf{u}}_\perp$ . For moderate values of  $N(l_\perp/H)$ , this term can account for local secondary flows ignited by the rotation of individual quasi-2D vortical structures [10]. Here, we shall on the contrary assume that  $N(l_\perp/H)$  and  $H/\delta \sim Ha$  are large enough to neglect it.

We are now only left with the wall friction  $\tau_W$  to model in order to complete our shallow water model. The latter is determined by the structure of the Hartmann boundary layer present along the channel walls, the stability of which is in turn determined by the Reynolds number scaled on its laminar thickness  $R = Ha/(2N) = Re/(2Ha)$ . In configurations where the bulk velocity is nearly uniform, it has been observed both in experiments [13] and numerical simulations [14] that the Hartmann

layer was laminar for  $R \lesssim 380$ . In this case, its profile is exponential and  $\tau_W$  takes the form of a linear friction term of dimensional characteristic time  $t_H = H^2/(\nu Ha)$ . The first 2D model for MHD flows, called SM82 after [5], essentially relies on this assumption. As announced in the introduction, our aim is to model quasi-2D flows where the Hartmann layer is turbulent. Although the general behaviour of the Hartmann layer may differ from that in idealised configurations with uniform bulk velocity, we may infer from this ideal case that the Hartmann layer is in a developed turbulent state whenever  $R$  significantly exceeds the ideal threshold value of 380. Several models exist for the turbulent Hartmann layer: while the early approaches of [21], [22] [23] and [24] attempted to incorporate the effect of the Lorentz force on turbulence within the layer, the authors of [15] more recently observed that even when electromagnetic forces were dominant in the core ( $N \gg 1$  in our notations), they were still smaller than inertia within the boundary layer when it was turbulent. This enabled them to derive a model for the non-dimensional total stress  $\tau(z, u^c)$  based on the usual Prandtl mixing-length model [25]. For a given value of the core velocity  $u^c$ , They showed that the non-dimensional stress profile  $\tau(z, u^c)$  across the Hartmann layer located at  $z = z_0$  was solution of an ODE, which, using stretched variable  $\xi = Ha|z - z_0|$ , could be written as:

$$\frac{\partial^2 \tau}{\partial^2 \xi^2} = \frac{2.5}{R(u^c)} \frac{\sqrt{\tau}}{\xi}, \quad (7)$$

$$\tau \left( \frac{11.3}{\tau_W(u^c) R(u^c)} \right) = \tau_W, \quad (8)$$

$$\lim_{\xi \rightarrow +\infty} \tau(\xi) = 0, \quad (9)$$

where  $R(u^c) = u^c H/(\nu Ha)$ . The unknown wall stress  $\tau_W(u^c) = \tau(z_0, u^c)$  is found by a shooting method. Figure 1 shows the variations of  $\tau_W(u^c)$  normalised by the laminar wall stress versus  $R$ , which is the unique parameter this ratio depends on. One sees that for  $R \simeq 1000$ , which corresponds to the regimes attained in the MATUR experiment, the turbulent Hartmann layer exerts as much as 2 to 3 times the friction of its laminar counterpart on the flow. Since Hartmann layer friction is almost the exclusive dissipation mechanism in the flow, the total angular momentum can be expected to drop by a similar factor below [8]'s prediction, which is based on a laminar Hartmann layer.

To implement this model for  $\tau_W$  in (1), we shall assume that  $u^c \simeq \bar{u}$  on the one hand, and that the validity of the model is not affected by the spatial or temporal variations of  $\bar{u}(x, y, t)$  and can therefore be applied locally on the other. The numerical solution of (7-9) yields a tabulated function  $\tau_W = g(\bar{u})$  which we shall use directly in (1).

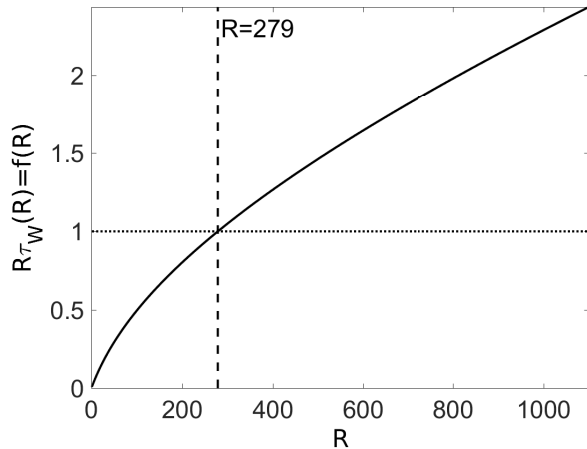


FIG. 1. Wall friction due to a turbulent (solid line) and laminar (dotted line) Hartmann layer, normalised by the latter, *vs.*  $R$ , the Reynolds number based on the Hartmann layer thickness and core (outer) velocity. This same ratio can also be expressed using dimensional quantities as  $\tilde{\tau}_W(U)t_H/(HU) = f(R)$ . It is equal to the ratio of laminar to turbulent friction times too.

Finally, our new 2D model consists of the set of equations:

$$\frac{N}{Ha^2} \nabla_{\perp}^2 \bar{\mathbf{u}}_{\perp} + \frac{N}{Ha} \left( \mathbf{u}_0 - \frac{2}{Ha} g(\|\bar{\mathbf{u}}_{\perp}\|) \frac{\bar{\mathbf{u}}_{\perp}}{\|\bar{\mathbf{u}}_{\perp}\|} \right) \quad (10)$$

$$\nabla \cdot \bar{\mathbf{u}} = 0, \quad (11)$$

where  $\mathbf{u}_0$  is built from the streamfunction  $\psi_0$ , solution of (5), which is uniquely determined by the electric boundary conditions of the problem.

### C. 2D model with a threshold for the friction

The model we just established assumes that the Hartmann boundary layers are everywhere turbulent. Although this assumption would seem reasonable in high speed duct flows, it is more questionable in flows in rotation, as in MATUR, where velocities are very low near the centre of rotation. This raises the much wider question of the spatial instability of the Hartmann layer: in a domain where regions of high velocity where  $R(\bar{u}) = \bar{u}H/(\nu Ha) > 380$  and regions of low velocity where  $R(\bar{u}) < 380$  coexist, can the Hartmann layer be turbulent in the former and laminar in the latter? Do, on the contrary, regions of turbulent Hartmann layers contaminate those of low velocity where the layer would otherwise be laminar? To our knowledge, these questions have not been studied. They certainly exceed the scope of our paper, as does the precise modelling of flows where such regions of high and low velocities coexist. Since, however, the state of the Hartmann layers may not always be known *a priori* in MATUR, we propose a variant to the

”all turbulent” model from section II B, where a threshold  $R_T$  on the value of the parameter  $R(\bar{u})$  based on the local velocity separates laminar from turbulent values of the friction:

$$\begin{aligned} \tau_W &= Ha \mathbf{u}_{\perp} \quad \text{for } R \leq R_T \\ \tau_W &= \frac{N}{Ha} g^{-1}(\|\mathbf{u}_{\perp}\|) \frac{\mathbf{u}_{\perp}}{\|\mathbf{u}_{\perp}\|} \quad \text{for } R > R_T \end{aligned} \quad (12)$$

In the forthcoming calculations, we set  $R_T$  either to the value of 279, at which turbulent friction matches laminar friction or of 380 at which Hartmann layers become turbulent in duct flows.  $R_T = 279$  is also close to the value at which turbulent Hartman layers re-laminarise [26]. Clearly, the value and the very existence of such a threshold do not take their origin in the actual physics of the flow. The main advantage of a model with threshold is that it is justified both in the limits of low velocities where the Hartmann layers are laminar everywhere and of high velocities where they are turbulent nearly everywhere.

## III. THE MATUR EXPERIMENT

### A. Problem geometry

We shall now describe the MATUR experiment which inspired the development of our model in the first place. The full detail of the experimental apparatus is reported in [2] and [27]. It consists of an airtight cylindrical container of radius  $\tilde{r}_0 = 11$  cm and depth  $H = 1$  cm entirely filled with mercury ( $\rho = 1.3529 \times 10^4$  kg.m<sup>-3</sup>,  $\nu = 1.1257 \times 10^{-7}$  m<sup>2</sup>.s<sup>-1</sup> and  $\sigma = 1.055 \times 10^6$   $\Omega^{-1}$ .m<sup>-1</sup>), and placed in the bore of a solenoidal magnet that maintains an homogeneous magnetic field of up to 6 T oriented along the cylinder axis  $\mathbf{e}_z$  (the ”tilde” indicates that quantities are dimensional). The frame origin is placed at the centre of the cylinder. Fluid motion is driven by connecting the positive pole of a DC electric current power supply to a large number of equally resistive electrodes mounted flush at the bottom wall along a circle of radius  $\tilde{r}_i = 5.4$  cm. The negative pole is connected to the electrically conducting circular side wall, while Hartmann walls, orthogonal to  $\mathbf{e}_z$  are electrically insulating, except at the locus of the current injection electrodes. A simplified sketch of the experiment is shown in figure 2. Under these conditions, the dimensional injected current density at the wall  $\tilde{j}_W$  is axisymmetric and may be modelled to a very good approximation as  $\tilde{j}_W = \delta_D(r - r_i)I/(2\pi\tilde{r}_i)$ , where  $I$  is the intensity of the total injected current and  $\delta_D$  is the Delta-Dirac distribution. Solving (5) as in [7] leads to the expression of the dimensional  $z$ -average of the Lorentz force:

$$\tilde{\mathbf{j}}_{\perp} \times \mathbf{B} = \rho \frac{\Gamma}{t_H} \mathcal{H}(\tilde{r} - \tilde{r}_i) \frac{1}{\tilde{r}}, \mathbf{e}_{\theta} \quad (13)$$

where  $\Gamma = I/(2\pi\sqrt{\sigma\rho\nu})$  is the total circulation induced by the current injection, and  $\mathcal{H}(r - r_i)$  is the Heaviside

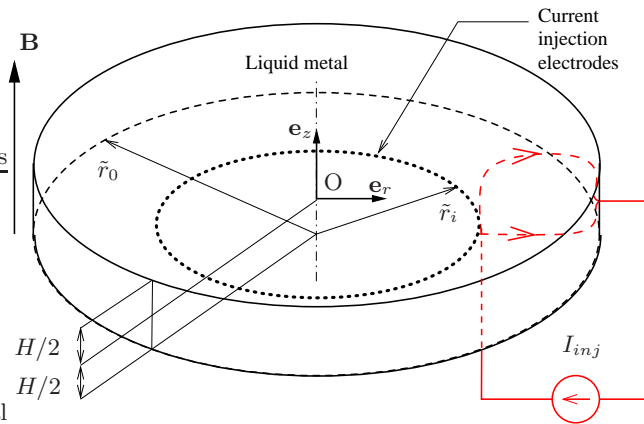


FIG. 2. Sketch of the Matur Experiment. A typical electric circuit including one of the point-electrodes mounted flush at the bottom Hartmann layer is represented in red. In reality, all electrodes located at  $r = r_i$  are connected.

step function. The problem geometry and the expression of the forcing suggest the choice of  $U = \Gamma/\tilde{r}_0$  as the reference velocity so that the forcing is expressed non-dimensionally in (10) as:

$$(\bar{\mathbf{j}}_{\perp} \times \mathbf{e}_z) = \mathbf{u}_0 = \frac{\tilde{r}_0}{H} \mathcal{H}(r - r_i) \frac{1}{r} \mathbf{e}_{\theta}. \quad (14)$$

(14) expresses that the electric current mostly flows radially in the Hartmann layers between  $r_i$  and  $r_0$  so the Lorentz force is azimuthal and acts almost exclusively in this region, and not within the disk  $r < r_i$  where the fluid isn't directly stirred. Initially, the MATUR experiment was indeed designed to study the circular shear layer that separates these two regions.

### B. An approximate expression for the Angular momentum in MATUR

Most of the viscous and Joule dissipation in quasi-2D flows under strong magnetic field takes place in the Hartmann layers. Whether these layers are laminar or turbulent therefore directly affects the global dissipation. In the MATUR experiment, this effect is best revealed through the relation between the total injected current and the global angular momentum. As a first application of our 2D model, we shall find an approximate relation between these two quantities under the simplified assumption that the flow is steady and axisymmetric. The total angular momentum can be expressed as:

$$L = \int_{\Omega} r u_{\theta}(r) d\Omega \quad (15)$$

$$= \int_{0 \leq r < r_i} r u_{\theta}(r) d\Omega + \int_{r_i \leq r \leq r_0} r u_{\theta}(r) d\Omega. \quad (16)$$

Since the most intense part of the flow takes place in the region  $r_i \leq r \leq r_0$ , where the forcing acts, we shall

neglect the contribution of the first integral to the total angular momentum. Then, by virtue of the mean value theorem, the second integral can be related to the azimuthal velocity at a point  $r_1$  such that  $r_i < r_1 < r_0$ :

$$L = \pi r_1 u_{\theta}(r_1) (r_0^2 - r_i^2). \quad (17)$$

The value of  $u_{\theta}(r_1)$  can be estimated using the azimuthal component of the Navier-Stokes equation (10), by noticing that outside the boundary layers, the forcing is mostly balanced by the Hartmann layer friction term:

$$u_{\theta}(r_1) \simeq g^{-1} \left( \frac{Ha}{2r_1} \right). \quad (18)$$

Since the radial profiles of azimuthal velocity measured in MATUR suggest that the local angular momentum  $r u_{\theta}(r)$  only slightly increases over  $r_i < r < r_0$  (this is confirmed by the radial profiles of azimuthal velocity obtained from numerical simulations on figure 6 and 7), we shall assume that  $r_1 u_{\theta}(r_1) \simeq r_0 u_{\theta}(r_0)$ . Using (17), an estimate for the total angular momentum can be expressed in terms of tabulated function  $g$  as:

$$L \simeq \pi (r_0^2 - r_i^2) g^{-1} \left( \frac{Ha}{2r_i} \right). \quad (19)$$

Note that in the case where the Hartmann layers are laminar, the SM82 model provides an explicit expression of the angular momentum for axisymmetric flows in MATUR as  $L_{SM82} = 4\pi(r_0^2 - r_i^2)$  [8]. The values of  $L$  obtained under this approximation and (19) are plotted on figure 3, along with the values of the angular momentum measured in MATUR for  $Ha = 132$  and  $Ha = 212$ . We have plotted the original dimensional data of [2] under the form of the angular momentum normalised by  $L_{SM82}$  vs.  $R$ . In these variables, experimental  $L(R)$  curves obtained at both values of  $Ha$  collapse well into a single curve. The most important feature of this curve is the rather sharp change of slope around  $R \simeq 380$ . For  $R < 380$ , the experimental values remain reasonably close to the SM82 linear approximation. By contrast, as soon as  $R > 380$ , they fall to significantly lower values than the linear prediction. This reveals a much higher level of dissipation in the flow than that induced by the laminar Hartmann friction, as would be expected when the Hartmann layers become turbulent. The value of  $R \simeq 380$  at which this transition occurs for both values of  $Ha$  brings support to this hypothesis. Even so, it is somewhat remarkable that the transition does take place roughly at the same value of  $R$  in such strongly different flows as channel flows with only one component of velocity such as the azimuthal flow studied by [13] or the rectilinear flow of [14] on one side, and that in MATUR on the other. The variations of  $L(R)$  calculated with our simplified axisymmetric model also support the hypothesis that the Hartmann layers become turbulent in MATUR when  $R \gtrsim 380$ , as it reproduces well the trend of the experimental values at large  $R$ : while  $L$  is overestimated by 10-20%, (19) exhibit nearly the same slope as

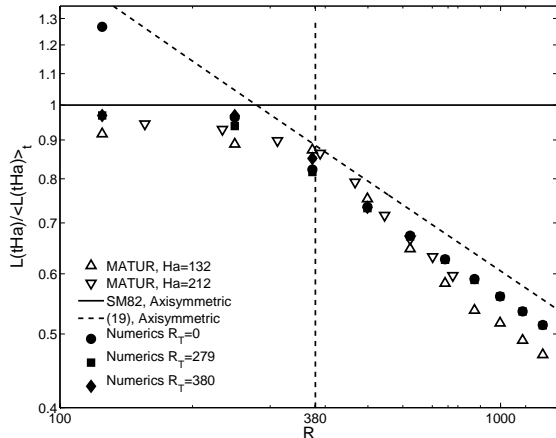


FIG. 3. Global angular momentum in MATUR for  $Ha = 132$  and  $Ha = 212$ . The axisymmetric approximation is obtained from (19). The critical value for the destabilisation of a plane Hartmann layer [13] is marked with a vertical dashed line.

the experimental curve. This level of discrepancy is similar to that found in regimes where the Hartmann layer is laminar between experimental values and the axisymmetric approximation based on SM82. Most importantly, for  $R > 380$ , where the model is supposed to be valid, (19) does reproduce the extra dissipation, while the linear model doesn't. Based on this encouraging result, we shall now lift the limitations of the axisymmetric assumption and attempt a more refined description of the flow based on 2D numerical simulations of our model.

#### IV. NUMERICAL SIMULATIONS OF THE MATUR EXPERIMENT

##### A. Numerical system and procedure

The numerical system we use to solve the 2D equations (10-11) in the MATUR geometry relies on commercial code FLUENT where the Finite Volumes method is implemented. The code differs very little from the one we previously used to simulate flows in the MATUR experiment at lower magnetic fields, and the meshes are identical. This earlier work is reported in [12], where the code is described in detail and extensively tested by following the procedure put forward by [28] to measure numerical convergence. Further tests on the same solver for the configuration of the flow past a cylinder can be found in [29]. To briefly summarise it, the spatial discretisation is of second order, upwind. The cases studied are unsteady and the time-scheme is a second order implicit pressure-velocity formulation. Within each iteration, the equations are solved one after the other (segregated mode) using the PISO predictor-corrector algorithm proposed by [30] to handle

$I / \text{A}$	10	20	30	40	50
$\Gamma / (2\tilde{r}_0) / \text{m/s}$	0.182	0.364	0.546	0.728	0.910
$2N$	11.71	5.85	3.90	2.93	2.34
$R$	125	249	374	499	623
time step $\times 10^{-4}$	2.5	2.6	5.3	4.0	5.3
$I / \text{A}$	60	70	80	90	100
$\Gamma / (2\tilde{r}_0) / \text{m/s}$	1.09	1.27	1.45	1.64	1.82
$2N$	1.95	1.67	1.46	1.30	1.17
$R$	748	872	997	1122	1247
time step $\times 10^4$	5.0	5.8	4.6	5.2	5.8

TABLE I. Dimensional and non-dimensional parameters for the 2D simulations of the MATUR experiment for  $Ha = 132$ . The non-dimensional time step is normalised by  $\Gamma^{-1}$ . It should be noted that the velocity estimate  $\Gamma / (2\tilde{r}_0)$  only gives an accurate estimate of the actual flow velocity when the Hartmann layer is laminar (this can be seen on figure 3). Turbulent dissipation in the Hartmann layer considerably reduces the latter for  $R > 380$ , so that in this regime,  $2N$ , which is an interaction parameter based on  $\Gamma / (2\tilde{r}_0)$  is noticeably lower than an interaction parameter that would be based on true values of the core velocity, and conditions (6) are comfortably satisfied.

the pressure-velocity coupling. The turbulent Hartmann friction term is treated explicitly at each iteration. The values of  $g(\|\mathbf{u}\|)$  are interpolated from a table that is pre-established by solving (7-9) for a discrete set of 1100 regularly spaced values of  $\|\mathbf{u}\|$ , between 0 and a maximum value of 0.8.

The mesh is made of quadrilateral elements, unstructured for  $r < 0.15$  and structured for  $0.15 < r < 1$ . The radial resolution is of 105 points, 25 of which are devoted to the boundary layer located at  $r = 1$ . These points are spread in the layer according to a geometric sequence of ratio 1.3 starting at  $r = 1$  with an initial interval of  $4.54 \times 10^{-5}$ . The azimuthal resolution is of 150 points. The time step is chosen so that the related cutoff frequency matches the spatial cutoff frequency for the maximum flow velocity (Courant-Friedrich-Lewy condition). The usual no-slip condition at the wall  $r = 1$  is applied. All calculated cases are listed in table I, with their corresponding non-dimensional parameters and time steps. The flow is initially at rest while the forcing is constant, given by (14) for  $t \geq 0$ .

Since the velocities involved in the cases simulated in the present work are considerably higher than those in [12], the suitability of our mesh (which we shall denote  $M_1$ ) was tested by comparing the numerical solution obtained with it for  $Ha = 132$  and  $R = 1122$  to one obtained with a mesh with the same structure, but where the resolution was doubled both in the radial and the azimuthal directions (mesh  $M_2$ ). The time-averaged global angular momentum and  $\mathcal{L}^2$  norm of the error on azimuthal velocities in the established state are gathered in table II. The relative discrepancy between the two solutions remains around 1% (see profiles on figure 7). In view of these results, we deem  $M_1$  suitable for the prob-

	$\frac{L}{L^{\text{SMSZ}}}$	$\frac{\ \langle u_\theta \rangle_t - \langle u_\theta^{(M_2)} \rangle_t\ _2}{\ \langle u_\theta^{(M_2)} \rangle_t\ _2}$
Mesh M <sub>1</sub>	0.5355	0.0198
Mesh M <sub>2</sub>	0.5375	0

TABLE II. Comparison between simulations performed on meshes M<sub>1</sub> and M<sub>2</sub> for  $Ha = 132$  and  $R = 1122$ .

lem we investigate.

### B. General aspect of the flow

The evolution of the flow is qualitatively similar to that found in our previous simulations of MATUR at lower  $Ha$ , where the current was injected closer to the wall (In [8] and [12],  $r_i/r_0 = 0.845$  and the Hartmann layer remained laminar.). Its main stages are represented by contours of vorticity on figure 4. At first, a laminar shear layer appears at  $r = r_i$  as the external corona  $r_i \leq r < r_0$  is driven in rotation. For all intensities of total injected current considered here, a threshold on the azimuthal velocity is very quickly reached where this circular free shear is subject to a Kelvin-Helmholtz instability that breaks it up into small vortices. These soon begin to merge into larger structures. They become distorted by the shear and the flow turns chaotic before it reaches a final turbulent state. Injecting the electric current at a lower radius than in the cases studied in [8, 12] introduces two differences: firstly, most large vortices and associated turbulent fluctuations remain relatively close to the centre of the domain, which unlike when  $r_i/r_0 = 0.845$ , is not still, but subject to a highly fluctuating fluid motion. Conversely, velocity fluctuations in the region near the outside cylinder wall are of much lower intensity. They result mostly from the tail of vortices generated near the injection electrodes that are stretched by the shear and conveyed outwards. The resulting flow in the outer region therefore exhibits long azimuthal vorticity streaks of much lower intensity than in the disk inside the circle of injection electrodes. Also, since large structures do not reach the outer wall, no flow separation occurs there. This wall has thus little influence on the flow, unlike in the two previously mentioned studies where the current was injected closer to it.

When the flow is well established, it goes through a recurring sequence. In the first phase, very strong vorticity emerges in segments along the circle where the current is injected (see figure 4,  $tHa = 2.34$ ). In the second phase, these fragile segments break up and roll into vortical structures ( $tHa = 2.41$ ). Those merge in the third phase to build up a small number of larger structures (at least two, as at  $tHa = 2.56$ ). These large structures progressively loose intensity as the cycle returns to the first phase.

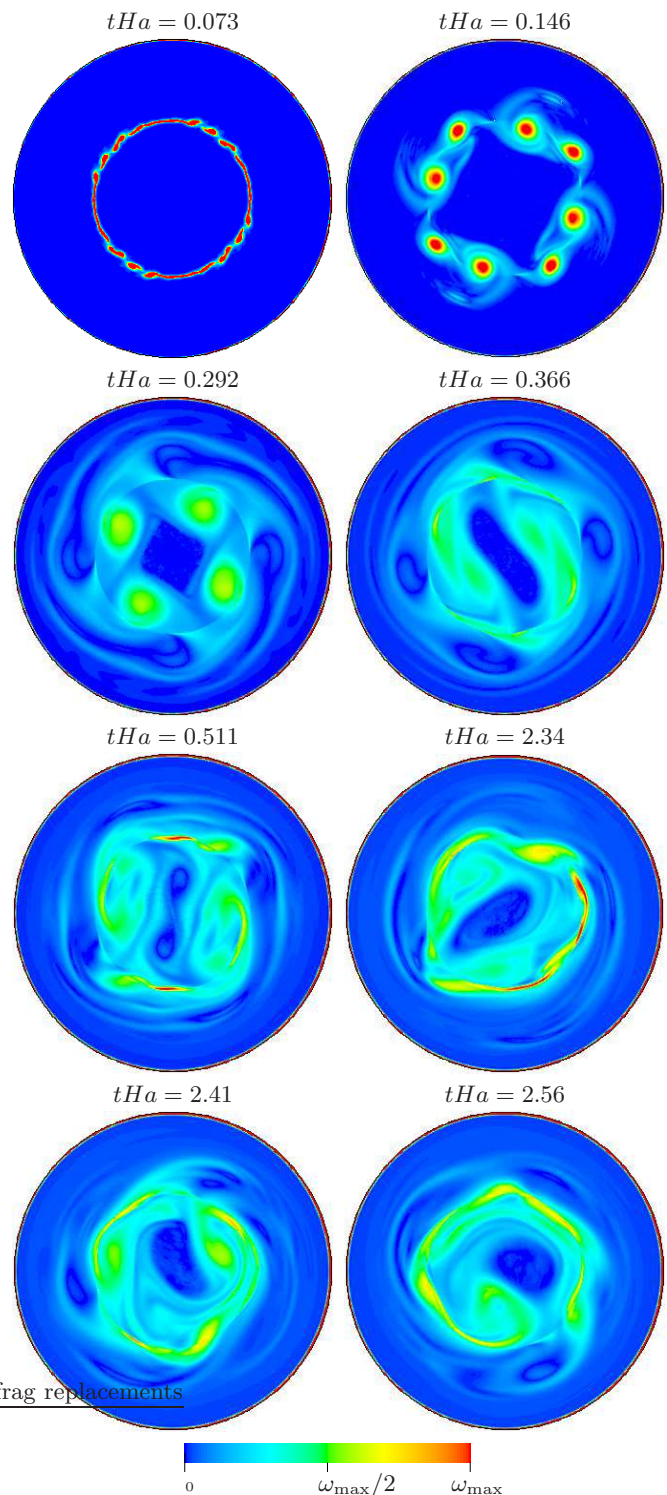


FIG. 4. Evolution of the flow from rest when the forcing is switched on for  $Ha = 132$  and  $R = 1122$ , obtained from numerical simulations based on the 2D model with  $R_T = 0$ .

### C. Global angular momentum

The presence of large vortices carried by the flow has a direct impact on the global angular momentum. Figure 3 indeed shows that the time averaged angular momentum computed in the established regime from the numerical simulations stands a little below the axisymmetric approximation of section III B, which ignored these large vortices. Remarkably, it stands on a curve that is closely parallel to that of the axisymmetric approximation but improves it by bringing the discrepancy to experimental values below 10% in the limit of large  $R$ . This remaining discrepancy may not even necessarily be attributed to the 2D model as [2] point out that metallic electrodes embedded in one of the rig's Hartmann walls precisely incur about 10% extra dissipation on the flow. Since this extra dissipation is not accounted for in either SM82 or PSM, the authors suggest that it may explain the discrepancy between experimental values and those obtained with SM82 in regimes where the Hartmann layer is laminar. It is thus reasonable to expect that the same mechanism is at play when the Hartmann layer is turbulent.

It is not surprising that the angular momentum predicted by the model that assumes a fully turbulent Hartmann layer ( $R_T = 0$ ) is significantly larger than the experimental values when  $R < 279$ . This discrepancy between numerical and experimental values then diminishes rapidly as soon as  $R \gtrsim 279$ . This reflects the behaviour of the mixing-length model for the turbulent Hartmann layer: as the Hartmann layer becomes more and more turbulent, it becomes more and more accurate. Numerical simulations based on the model with  $R_T = 279$  become very close indeed to those from the model based on a fully turbulent Hartmann layer in the limit of large  $R$ . Additionally, the model with  $R_T = 279$  performs a lot better than that with  $R_T = 0$  in the limit of small  $R$  where the Hartmann layers are laminar everywhere. In this last case, the model coincides with the SM82 model which slightly overestimated the angular momentum, compared to the experiment, as noted by [8]. When  $R$  is of the order of 380 the model with threshold reproduces well the saturation observed in the experiment. Considering that the dissipation incurred by the metallic electrodes should imply that experimental values be a little lower than those returned by the model (as for large  $R$ ), we must conclude that both models with  $R_T = 0$  and  $R_T = 279$  overestimate the dissipation by around 10% in this transitional regime.

Finally, a handful of cases with  $R_T = 380$  were computed and they were found to differ very little from those at  $R_T = 279$ , apart from a slightly better performance in the transitional regime. This is certainly an indication that the transitional regimes involve more complex mechanisms than a local threshold on the local friction.

The time variations of the global angular momentum

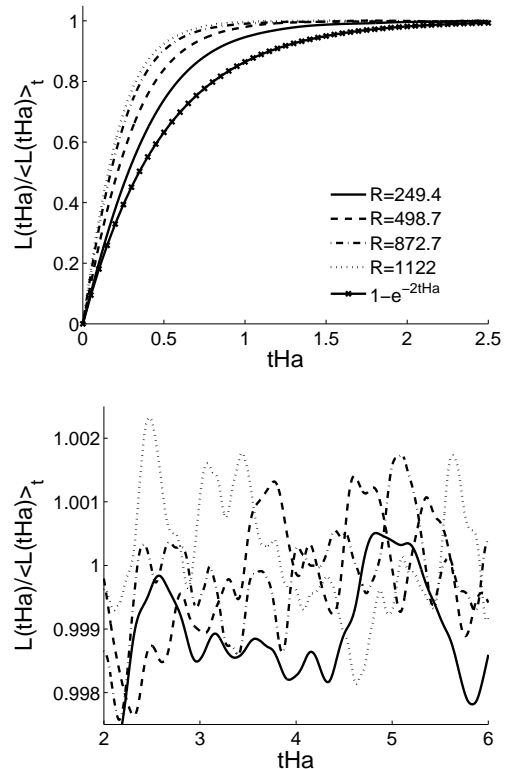


FIG. 5. Relative time-variations of the global Angular momentum in MATUR under constant forcing, obtained from the model with  $R_T = 0$ . Top: "spin-up" transient with the fluid initially at rest. The theoretical evolution of  $L$  according to SM82 (axisymmetric) is represented to illustrate how turbulent friction shortens the flow reaction time. Bottom: fluctuations in the established regime.  $tHa$  is the non-dimensional time normalised by the Hartmann friction time, while  $\langle \cdot \rangle_t$  stands for time averaged quantities in the established state.

reveal a further two properties of the flow. Firstly, figure 5 (top) shows that the transient time required to bring the flow from rest to an established state decreases with  $R$ , for  $R_T = 0$ . This contrasts with quasi-2D flows with laminar Hartmann layers where the dimensional linear friction time  $t_H$  is independent of the flow intensity. Secondly, the flow in the established regime exhibits erratic fluctuations of global angular momentum of a relative intensity that remains around 0.3% through the range of parameters spanned here. Fluctuations of similar amplitude were found in numerical simulations of MATUR performed with the SM82 model in cases where the Hartmann layers were laminar [12]. Thus, although the turbulent Hartmann layer produces a lot more dissipation than its laminar counterparts, it doesn't eliminate the oscillations of the quasi-2D angular momentum, as the PSM model does.

#### D. Radial profiles of azimuthal velocity

The radial profiles of time-averaged azimuthal velocity in the established regime (figures 6 and 7) confirm the conclusions reached when analysing the global angular momentum: the discrepancy between experimental and numerical profiles decreases as  $R$  increases and the Prandtl model becomes more accurate. For  $R \gtrsim 700$ , the error can hardly be distinguished from the experimental error. Even so, it seems that the turbulent model slightly underestimates azimuthal velocities in the central region for the larger values of  $R$ . Furthermore, even in the most turbulent cases analysed here, the parameter  $R(\Gamma/(2\tilde{r}_0))$  which is based on the linear estimate for the velocity  $\Gamma/(2\tilde{r}_0)$ , is of 1247. In this case, the actual maximum velocity in the flow is about half of  $\Gamma/(2\tilde{r}_0)$ , so a more realistic value of  $R$  would be around 600, which is only mildly supercritical. Considering this, the performances of the 2D model are excellent. Furthermore, it can be noticed that there are only few experimental points in the vicinity of the wall at  $r = r_0$ . Since this region brings the highest contribution to the global angular momentum, the experimental error there might also be in part responsible for the residual difference in angular momentum at high  $R$  between our model and the experiment. In spite of this minor uncertainty, the fact that both global and local quantities measured in MATUR are closely recovered over a wide range of parameters by the numerical simulations of our model is certainly a good evidence that the extra dissipation observed at  $Ha = 132$  and  $Ha = 212$  is indeed due to the turbulent state of the Hartmann layers.

The models with  $R_T = 279$  and  $R_T = 380$  improve on that with  $R_T = 0$  in that they very accurately render regimes where the Hartmann layer is laminar (case  $R = 249.4$ ). In the transitional regime around  $R = 380$ , even though both models are able to reproduce the curve  $L(R)$ , they underestimate the actual velocity of the flow by up to 15% in the outer region  $r_i \leq r \leq r_0$  (see figure 6 for  $R = 374$  and  $R = 498.7$ , for which the discrepancy between models and experiment is most conspicuous). For  $R = 374$ , the model with  $R_T = 380$  yields higher velocities in the vicinity of the outer wall at ( $r = r_0$ ) than that with  $R_T = 279$ , because the value of  $\bar{u}$  such that  $R(\bar{u}) = 380$  is reached between  $r_i$  and  $r_0$ . When only a small part of the flow is subject to turbulent friction (case with  $R = 249.4$ ), the model with  $R_T = 380$  performs better than that with  $R_T = 279$ . This is an evidence that the Hartmann layer is almost entirely laminar in the experiment in this regime. Since with a threshold of  $R_T = 380$ , only a very narrow region around  $r/r_0 \simeq 0.6$  experiences turbulent friction, this value of  $R_T$  turns out to yield more realistic results than  $R_T = 279$ . As expected, for higher values of  $R$ , the profiles of velocity and velocity fluctuations obtained with  $R_T = 279$  and  $R_T = 380$  with threshold depart little from the model with  $R_T = 0$ . The profiles obtained from both models with threshold differ even less from each other, to the point where they can't

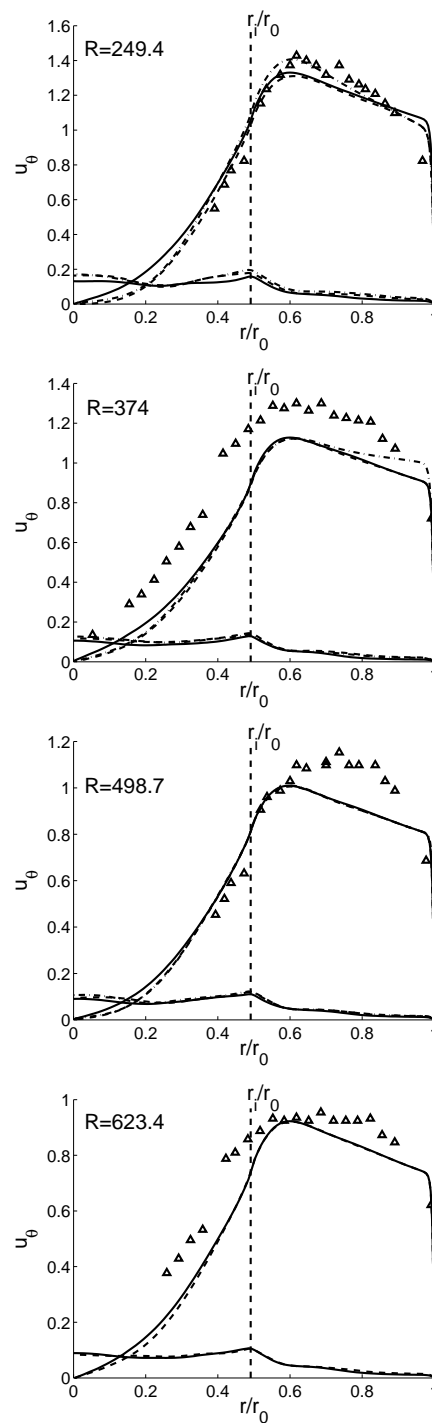


FIG. 6. Radial profiles of mean azimuthal velocity and RMS fluctuations of azimuthal velocity (set of curves with values around 0.1). Legend is on figure 7.

be distinguished on the graph. Overall, the model with  $R_T = 380$  can be deemed valid whenever  $R \lesssim 300$  or  $R \gtrsim 600$ .

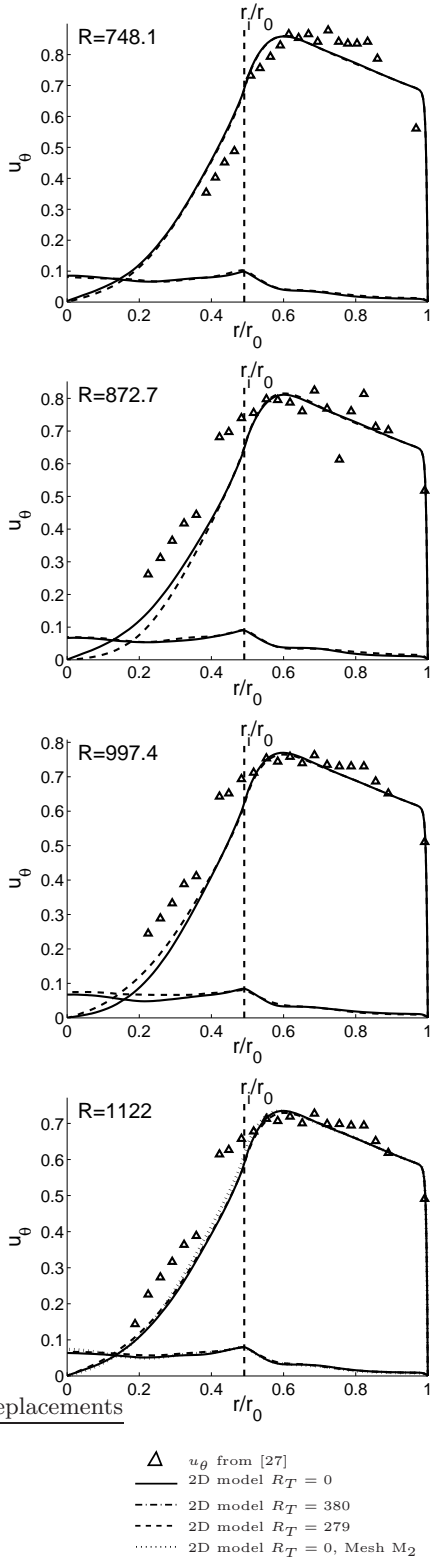


FIG. 7. Radial profiles of mean azimuthal velocity and RMS fluctuations of azimuthal velocity (set of curves with values around 0.1). Comparison between experimental, numerical results obtained with the models with threshold, without threshold, and on mesh  $M_2$  (for  $R = 1122$  only).

## E. Velocity fluctuations

The RMS averages of absolute azimuthal velocity fluctuations are reported on figures 6 and 7 and their relative counterpart are gathered on figure 8 (top). All curves exhibit a more or less triangularly shaped maximum at the location of the current injection electrodes. This reflects the passage of the large structures that result from the merging of small vortices generated by the instability of the circular free shear layer at  $r = r_i$ . The width of the triangle gives an idea of the size of these structures. In all cases, fluctuations are significantly higher in the region  $r < r_i$  than for  $r > r_i$ . This indicates that, as seen from the contours of vorticity on figure 4, once released from their region of origin, these large structures drift towards the centre of the domain rather than towards the external wall, unlike in cases where  $r_i/r_0 = 0.84$  [12]. The shape of the profile remains the same when  $R$  increases, while the relative intensity of the fluctuations decreases only slightly. We shall see thereafter that this behaviour mostly results from the competition between a more intense flow, which drives more intense relative velocity fluctuations and the turbulent Hartmann friction, which damps them. Indeed, the latter increases several times more than its laminar counterpart with the flow intensity.

The radial profiles of the relative correlation between radial and azimuthal velocity fluctuations shown on figure 8 (bottom) give a good measure of the turbulent intensity. The general aspect of these curves presents some interesting features: for  $r < r_i$ , where  $\langle u_\theta^2 \rangle^{1/2}$  keeps relatively high values, the correlations drops to zero. Conversely, in the region  $r > r_i$ , where  $\langle u_\theta^2 \rangle^{1/2}$  dropped, the correlations exhibit a moderately high, positive value. This reflects the difference in the nature of turbulence between these two regions already noted in section IV B: for  $r < r_i$ , fluctuations are fed by large structures drifting to the centre. By contrast, fluctuations in the outer region ( $r > r_i$ ) are the trace of azimuthal streaks of vorticity that originate from the tail of the large structures. These are stretched by the shear and transported outwards.

Furthermore, the correlations of relative radial and azimuthal velocity fluctuations decrease more noticeably with  $R$  than the RMS velocity fluctuations (this is partly due to the former being a quadratic function of the velocity, while the latter are linear). They then stabilise at nearly the same value for  $R \gtrsim 997$ . This diminution of turbulence intensity reflects that the turbulent Hartmann layer friction, which increases non-linearly with  $R$ , absorbs an ever increasing fraction of the energy injected in the flow at the expense of quasi-2D turbulent fluctuations.

This nonlinear variation of  $\tau_W$  with  $R$  also explains that the region characterised by negative correlations or by the triangular-shaped maximum of RMS velocity fluctuations doesn't appreciably increase in size with  $R$ . If anything, it even slightly narrows. Since it is essentially

determined by passing large structures, this phenomenon can be understood by noticing that the size of these structures is limited by boundary layer friction: if  $U_L$  is the typical self rotation velocity of a vortex of size  $L^{\text{turbulent}}$  (*resp.*  $L^{\text{laminar}}$ ) when the Hartmann layers are turbulent (*resp.* laminar), then any vortex with a turnover time  $L^{\text{turbulent}}/U_L$  (*resp.*  $L^{\text{laminar}}/U_L$ ) higher than the typical Hartmann layer friction time is dissipated [31]. This determines their scaling as:

$$\begin{aligned} \frac{L^{\text{turbulent}}}{H} &\sim \frac{R}{f(R)} \left(\frac{U_L}{U}\right)^{\text{turbulent}} \\ &\leq \frac{R}{f(R)} \left(\frac{U_L}{U}\right)^{\text{laminar}} = \frac{1}{f(R)} \frac{L^{\text{laminar}}}{H} \\ &< \frac{L^{\text{laminar}}}{H}. \end{aligned} \quad (20)$$

For turbulent Hartmann layers,  $f(R)$  is greater than unity and increases monotonically (see figure 1). Furthermore, since  $U_L/U$  is roughly the intensity of the azimuthal velocity fluctuations, it decreases a little with  $R$  and it is smaller when the Hartmann layers are turbulent than when they are laminar. The scaling (20) thus shows that the increasing turbulent friction opposes the increase in size of the large scales with  $R$  and that those are therefore smaller than when the Hartmann layers are laminar. This explains why the region where  $\langle u'_r u'_\theta \rangle$  is negative doesn't widen with  $R$ . It also explains that the thickness of the free shear layer at  $r = r_i$ , which the large structures conveyed by the flow also determine, remains seemingly unchanged as  $R$  increases (This can be seen on figures 6 and 7). By contrast, [2] found that when Hartmann layers were laminar, and boundary layer friction was less intense, the thickness of this layer slowly increased as  $R^{1/2.2}$ .

Finally, it should be noted that both types of fluctuations obtained with the model at  $R_T = 279$  exhibit essentially the same behaviour as those from the model at  $R_T = 0$ .

## V. CONCLUSION

We have established a 2D model that applies to channel flows under transverse magnetic fields with turbulent Hartmann layers. Numerical simulations of the MATUR experiment based on it gave strong evidence that the previously unexplained level of dissipation observed at  $Ha = 132$  and  $Ha = 212$  was caused by turbulence in the Hartmann layers.

Unlike its predecessors, which account for laminar Hartmann layers, the new model is not rigorously derived from first principles but relies instead on the equations for the Hartmann layer friction based on Prandtl's assumption proposed by [15]. Nevertheless, as soon as the Reynolds number based on the Hartmann layer thickness exceeds about 600, 2D numerical simulations of this model reproduce the experimental results from [2] with discrepancies below 10% on the global angular

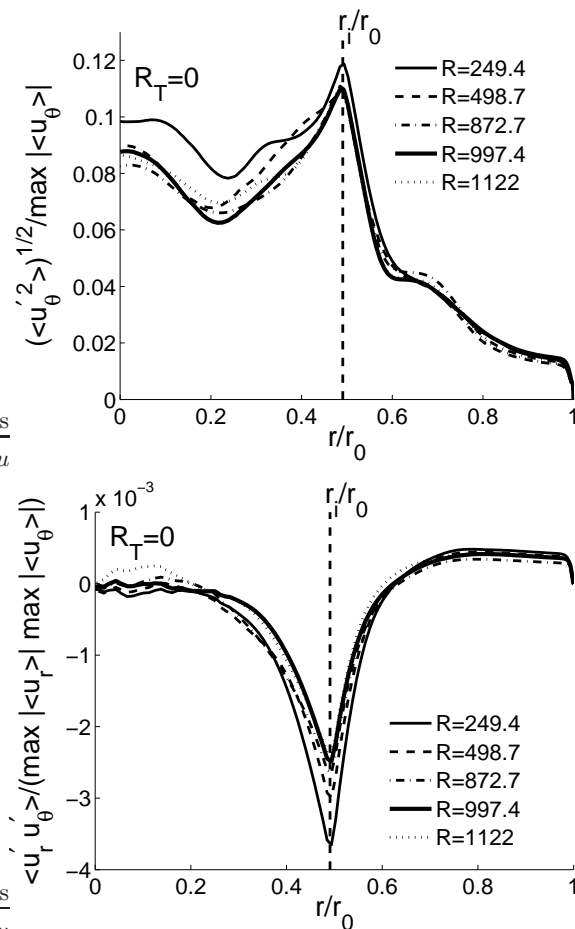


FIG. 8. RMS of relative azimuthal velocity fluctuations (top) and correlations of azimuthal and radial velocity fluctuations, normalised by maximum average velocities (bottom). Both graphs were obtained from simulations of the 2D model with  $R_T = 0$ .

momentum and an error on local velocities that falls within the experimental error. The parametric analysis for  $124 < R < 1247$  performed in this work reveals that the precision of the model increases with  $R$ , a feature it inherits from [15]'s and Prandtl's models. This sheds an even better light on the precision of the results obtained here, since in terms of the velocity actually achieved in the flow, the highest value of  $R$  reached here barely exceeded 600, which according to the work of [13] is only mildly supercritical, in terms of the transition to turbulence in the Hartmann layer.

We have also introduced an admittedly artificial variant of our model where the boundary layer friction reverted to its laminar value below a threshold value of  $R_T$ .  $R_T$  was tuned either to 279, value at which laminar and turbulent frictions coincide, or to the value of 380 found by [13] and [14] for the transition to turbulence in the Hartmann layers in a rectilinear channel flow. Although the models with thresholds cannot precisely render the transitional regimes  $300 \lesssim R \lesssim 600$  where neither of

the 2D models based on fully laminar or fully turbulent Hartmann layers are meant to operate, they gather these two models in a single one. The results obtained with either thresholds don't differ a great deal, although only the model with  $R_T = 380$  recovers well the experimental values of the global angular momentum, even in transitional regimes of the Hartmann layers ( $R \simeq 380$ ). Threshold models therefore constitute a useful extension of the fully turbulent model, particularly for flows where the state of the Hartmann layers may not be known *a priori*.

Despite not sharing the asymptotic pedigree of their predecessors (SM82 and PSM), the new class of shallow water models we introduced not only offers the same flexibility and simplicity but also the same level of performance. In this regard, it makes it now possible to simulate flows as complex as those in MATUR, where both three-dimensional boundary layer turbulence and quasi-2D turbulence coexist a low computational cost. This was previously not possible with either SM82 or

PSM since these models are restricted to flows where Hartmann layers are laminar. These new models now make extensive parametric analyses of a wide new class of flows with turbulent Hartmann layers easily accessible. Such an analysis would indeed incur very large computational costs if carried out with 3D simulations where the Hartmann layer would be meshed.

It is precisely such a parametric analysis that has allowed us to reveal two important properties of quasi-2D flows with turbulent Hartmann layers: firstly, turbulent friction restricts the size of the large scales, compared to its laminar counterpart. Secondly, it has a stabilising effect on the quasi-2D flow, as it dissipates an increasingly high fraction of the 2D turbulent energy when the flow is driven more intensely.

The authors are grateful to Thierry Alboussière and Pablo Moresco for their fruitful input during the conduct of this work. They are also grateful to referee 2, whose remarks have greatly helped to improve the precision of the models.

- 
- [1] T. Alboussière, V. Uspenski, and R. Moreau. Quasi-2D MHD turbulent shear layers. *Experimental Thermal and Fluid Science*, 20(20):19–24, 1999.
- [2] K. Messadek and R. Moreau. An experimental investigation of MHD quasi-two-dimensional turbulent shear flows. *J. Fluid Mech.*, 456:137–159, 2002.
- [3] B. Lehnert. An instability of laminar flow of mercury caused by an external magnetic field. *Proc. R. Soc. Lond. A*, 233:299–302, 1955.
- [4] P. H. Roberts. *Introduction to Magnetohydrodynamics*. Longmans, 1967.
- [5] J. Sommeria and R. Moreau. Why, how and when MHD turbulence becomes two-dimensional. *J. Fluid Mech.*, 118:507–518, 1982.
- [6] J. Pedlosky. *Geophysical Fluid Dynamics*. Springer Verlag, 1987.
- [7] J. Verron and J. Sommeria. Numerical simulations of a two-dimensional turbulence experiment in magnetohydrodynamics. *Phys. Fluids*, 30:732–739, 1987.
- [8] Y. Delannoy, B. Pascal, T. Alboussière, V. Uspenski, and R. Moreau. *Quasi-Two-Dimensional Turbulence in MHD Shear Flows: The MaTur Experiment and Simulations*. Kluwer, A. Alemany et al. edition, 1999.
- [9] B. Sreenivasan and T. Alboussière. Experimental study of a vortex in a magnetic field. *J. Fluid Mech.*, 464:287–309, 2002.
- [10] A. Pothérat, J. Sommeria, and R. Moreau. An effective two-dimensional model for MHD flows with transverse magnetic field. *J. Fluid Mech.*, 424:75–100, 2000.
- [11] S. Smolentsev and R. Moreau. One-equation model for quasi-two-dimensional turbulent magnetohydrodynamic flows. *Phys. Fluids*, 19:078101, 2007.
- [12] A. Pothérat, J. Sommeria, and R. Moreau. Numerical simulations of an effective two-dimensional model for flows with a transverse magnetic field. *J. Fluid Mech.*, 534:115–143, 2005.
- [13] P. Moresco and T. Alboussière. Experimental study of the instability of the Hartmann layer. *J. Fluid Mech.*, 504:167–181, 2004.
- [14] D. Krasnov, E. Zienicke, O. Zikanov, T. Boeck, and A. Thess. Numerical study of the instability of the Hartmann layer. *J. Fluid Mech.*, 504:183–211, 2004.
- [15] T. Alboussière and R. J. Lingwood. A model for the turbulent Hartmann layer. *Phys. Fluids*, 12(6):1535–1543, 2000.
- [16] A. Pothérat, J. Sommeria, and R. Moreau. Effective boundary conditions for magnetohydrodynamic flows with thin Hartmann layers. *Phys. Fluids*, pages 403–410, 2002.
- [17] R. Moreau. *Magnetohydrodynamics*. Kluwer Academic Publisher, 1990.
- [18] R. Klein, A. Pothérat, and A. Alferjonok. An experiment on an electrically driven, confined vortex pair. *Phys. Rev. E*, 79(1):016304, 2009.
- [19] R. Klein and A. Pothérat. Appearance of three dimensionality in wall-bounded MHD flows. *Phys. Rev. Lett.*, 104(3):034502, 2010.
- [20] A. Kljugin and A. Thess. Direct measurement of the stream-function in a quasi-two-dimensional liquid metal flow. *Exp. Fluids*, (25):298–304, 1998.
- [21] L. P. Harris. *Hydromagnetic Channel Flows*. The Technology Press of the MIT, 1960.
- [22] G.G. Branover. Resistance of magnetohydrodynamic channels. *Magnetohydrodynamics*, 3(1), 1967.
- [23] P.S. Lykoudis. Transition from laminar to turbulent flow in magnetofluid mechanic channels. *Rev. Mod. Phys.*, 79:797, 1960.
- [24] P.S. Lykoudis and E.C. Brouillette. Magneto-fluid-mechanics channel flows ii: Theory. *Phys. Fluids*, 10:1002, 1967.
- [25] H. Schlichting. *Boundary Layer Theory*. Mc Graw Hill, 1955.

- [26] R. J. Lingwood and T. Alboussière. On the stability of the Hartmann layer. *Phys. Fluids*, 11:2058–2068, 1999.
- [27] K. Messadek. *Une Expérience Sur La Turbulence MHD Quasi-Bidimensionnelle*. PhD thesis, Institut National Polytechnique de Grenoble, 2001.
- [28] P. J. Roache. Quantification of uncertainty in computational fluid dynamics. *Ann. Rev. Fluid Mech.*, 29:123–60, 1997.
- [29] V. Dousset and A. Pothérat. Numerical simulations of a cylinder wake under strong axial magnetic field. *Phys. Fluids*, page 017104, 2008.
- [30] R. I. Issa. Solution of the implicitly discretized fluid flow equations by operator-splitting. *J. Comp. Phys.*, 62:40–65, 1986.
- [31] M. Chertkov, C. Connaughton, I. Kolokolov, and V. Lebedev. Dynamics of condensation in two dimensional turbulence. *Phys. Rev. Lett.*, 99:084501, 2007.